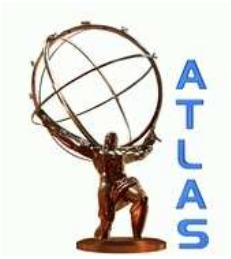

ATLAS NOTE

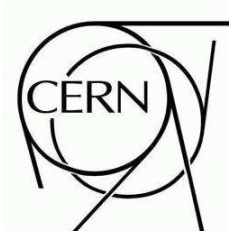

11th March 2009

Dilepton Resonances at High Mass

The ATLAS Collaboration[1)]

This note is part of CERN-OPEN-2008-020. This version of the note should not be cited: all citations should be to CERN-OPEN-2008-020.

ATL-PHYS-PUB-2009-070
10 May 2009

Abstract

We present the discovery potential of a heavy new resonance decaying into a pair of leptons with early LHC data with the ATLAS detector. The dilepton final states are robust channels to analyze because of the simplicity of the event topology. The unprecedented available center-of-mass energy will allow one to probe regions that are inaccessible at previous experiments even with modest amounts of data. After studying the Standard Model predictions and the associated uncertainties one can then look for significant deviations as indication of beyond the Standard Model physics (BSM). The focus of the note is to study the prospects for discovering BSM physics in the dilepton final states with an integrated luminosity ranging from 100 pb^{-1} to 10 fb^{-1}.

[1)]This note prepared by F.M.L. Almeida jr, X.S. Anduaga Del Popolo, A. Antonaki, H. Bachacou, T. Berry, K. Black, J. Butler, E. Castaneda Miranda, Z. Czyczula, K. Dindar, M.T. Dova, D. Fassouliotis, S. Ferrag, L. Flores Castillo, C. Guyot, H. Hadavand, F. Heinemann, C. Helsens, R. Kehoe, C. Kourkoumelis, J.-F. Laporte, F. Ledroit-Guillon, J. Love, J. Morel, A.A. Nepomuceno, A. Ouraou, J. Parsons, M. Tamsett, E.N. Thompson, A. De Santo, T. Vickey, S. Willocq, S.L. Wu, N. Zhou.

1 Introduction

New heavy states forming a narrow resonance decaying into opposite sign dileptons are predicted in many extensions of the Standard Model: grand unified theories, Technicolor, little Higgs models, and models including extra dimensions [1–4]. The discovery of a new heavy resonance would open a new era in our understanding of elementary particles and their interactions. Because of the historic importance of the dilepton channel as a discovery channel and the simplicity of the final state, these channels will be very important to study with early ATLAS data. The strictest direct limits on the existence of heavy neutral particles are from direct searches at the Tevatron [5–7]; the highest excluded mass is currently almost 1 TeV. The LHC will have a center-of-mass energy of 14 TeV which should ultimately increase the search reach for new heavy particles to the 5 - 6 TeV range. Many exotic models can be tested at the LHC, but analyzing all the existing models is impossible. Instead we choose to take a different approach, grouping the early-data analysis by their final state topologies. There have been several other ATLAS studies evaluating the potential for discovery of a heavy resonance [8]. However, this is the first study to include full trigger simulation, misalignments, and data driven methods. Including these experimental issues is important to realistically estimate the analysis potential. We focus on the early data phase of the experiment, defined roughly to include the accumulation of up to 10 fb^{-1} of ATLAS data.

In the remaining of this introduction, the investigated models are reviewed. In sections 2 and 3, we explore the detector performance concerning the electron, muon and tau reconstruction abilities at high energies and the corresponding trigger efficiencies. In section 4 we investigate the Standard Model predictions and associated uncertainties, as well as the signal cross-section. In section 5, we proceed to search for Exotic resonances.

1.1 Models Predicting a Z'

Several models [1,3] predict the existence of additional neutral gauge bosons. In particular, grand unified theories, as well as "little Higgs" models, predict their existence as a manifestation of an extended symmetry group. Generically, there are no predictions for the mass of these particles. Since the experimental consequences are very similar in the dilepton final state, we examine only some representative models: the Sequential Standard Model (SSM)[2)], the E_6 and the Left-Right Symmetric models [9]. The partial width of the Z' boson is given by $\Gamma(Z' \to \ell^+\ell^-) \approx [(g_\ell^R)^2 + (g_\ell^L)^2]\frac{m_{Z'}}{24\pi}$ where g_ℓ^R and g_ℓ^L are the right and left handed couplings of the charged leptons to the Z' boson and $m_{Z'}$ is the mass of the Z' boson. For the masses and couplings considered here the natural width is typically around 1% of the mass of the resonance.

The strictest limits from direct searches come from the D0 and CDF experiments at the Tevatron [5–7]. Indirect searches have also been undertaken by the LEP experiments [10]. The direct limits range from several hundred GeV to approximately 1 TeV and are shown in Table 1. These limits are not expected to improve much beyond 1 TeV [11]. It should be noted that for models where the Z' couples preferentially to the third generation the limits are lower, therefore we consider it important to look at a lower invariant mass region in this channel.

1.2 Randall-Sundrum Graviton

The Randall-Sundrum model [4] addresses the hierarchy problem by adding one extra-dimension linking two branes, the Standard Model brane and the Planck brane. The hierarchy is solved by assuming for the fifth dimension a warped geometry in which the size of the ordinary coordinates decreases exponentially from the Planck scale to the TeV scale. The Randall-Sundrum model predicts the existence of a tower

[2)] The Sequential Standard Model includes a new heavy gauge boson with exactly the same couplings to the quarks and leptons as the Standard Model Z boson.

Z' Model	Indirect Searches (GeV)	Direct Searches (GeV)	
		e^+e^- Colliders	p^+p^- Colliders
Z'_χ	680	781	864
Z'_ψ	481	366	853
Z'_η	619	515	933
Z'_{LRSM}	804	518	–
Z'_{SSM}	1787	1018	966

Table 1: 95% C.L. limits on various Z' models.

of Kaluza-Klein excitations of the graviton. These should be observable as resonances which decay into lepton pairs at the LHC. The current limits depend on the parameters of the model, and range from several hundred GeV to one TeV [5]. We consider the observability of a Randall-Sundrum graviton decaying into electron pairs. The width of the graviton resonance would be very small. For the parameters considered here it ranges from 10^{-4} to a few 10^{-3} times the mass.

1.3 Technicolor

Strongly interacting theories, like Technicolor and Extended Technicolor, provide a dynamical solution to the problem of Electroweak Symmetry Breaking. Many new technifermions which are bound together by a QCD-like force are predicted. One of the most promising search channels is the dilepton decay of the ρ_{TC} and ω_{TC}. We study the "Technicolor Strawman Model" or TCSM [12, 13] as a benchmark model for generic strongly interacting theories. The most stringent limits on technihadrons in the TCSM framework come from the CDF collaboration, who rules out ρ_{TC} and ω_{TC} with masses below 280 GeV for a particular choice of the TCSM parameters [14]. The width of the techni-mesons depends on the number of technicolors, but is generally assumed to be small, of the order of a few percent of their mass. More details on the exact values of the parameters considered are discussed in a later section.

2 Object Identification and Performance

This section describes the requirements used to select objects for the analyses and summarizes findings on the performance using Monte Carlo simulations of the production and decay of new dilepton resonances.

2.1 Electron Identification

The electron identification and performance is described in detail elsewhere [15]; here we summarize the results concerning very high transverse momentum[3)] (p_T). electron identification and reconstruction. The background to very high p_T electron pairs is expected to be low, therefore only minimal selection criteria need to be applied, in order to maximize efficiency. These minimal criteria are called *loose*. On the other hand, when trying to select very high p_T τ lepton pairs, where one τ decays hadronically, a tighter selection on the electron from the other τ decay is needed.

On top of the minimal requirements that the reconstructed clusters should have an absolute pseudo-rapidity (η) less than 2.5 and should be associated with a track reconstructed in the inner detector, two electron selections were studied (both described in detail in [15]):

- A *loose* selection based on hadronic leakage and shower shape variables. This selection achieves very high efficiency while maintaining rejection against highly energetic pions with wide showers.

[3)] The transverse momentum is defined as the momentum projected on the plane transverse to the beam axis.

- A *medium* selection, which makes further requirements to obtain better rejection against $\pi^0 \to \gamma\gamma$ background by exploiting the very fine granularity of the first compartment of the electromagnetic calorimeter, and tighter requirements on the associated track.

Figure 1 shows the reconstruction efficiency together with the efficiency of the two selections in a sample $Z' \to e^+e^-$ events with $m_{Z'} = 1$ TeV as a function of transverse momentum and pseudo-rapidity, normalized to truth electrons with p_T greater than 50 GeV and $|\eta|$ smaller than 2.5. The efficiency of the reconstruction is dominated by the efficiency of the cluster to track association and is on average slightly below 80%. It must be noted that this efficiency has improved in the more recent software version used in [15]. The *loose* selection criteria have a relative efficiency close to 1, whereas the *medium* selection leads to an overall average efficiency between 65% and 70%.

The energy resolution for electrons at high p_T is about 1% except in the crack region between the forward and central calorimeters where the resolution is about 5% . The probability to assign the wrong charge to an electron ranges from 1% to at most 5% as the transverse momentum goes from 100 GeV to 1 TeV [16]. For a 1 TeV Z' a dielectron mass resolution of $(0.80 \pm 0.02)\%$ is obtained.

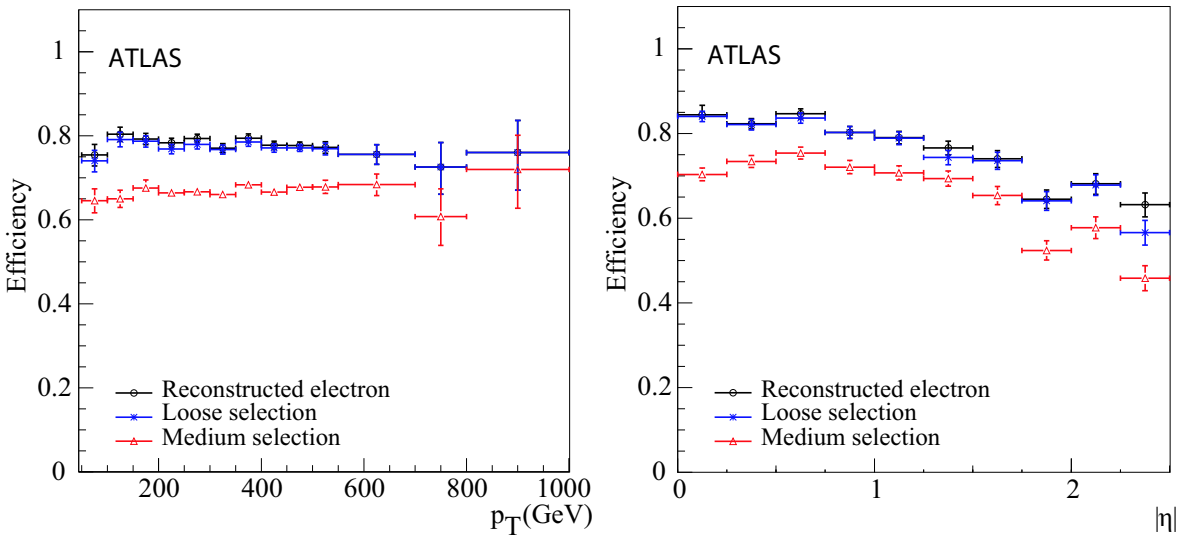

Figure 1: Efficiency of the *loose* and *medium* selection criteria in $Z' \to e^+e^-$ events with $m_{Z'} = 1$ TeV as a function of p_T (left) and η (right). The reconstruction efficiency is normalized to truth electrons inside the geometrical acceptance $|\eta| < 2.5$ and with $p_T > 50$ GeV.

2.2 Muon Identification

Here we discuss the requirements used to select muons, as well as a method to extract the identification efficiency from data. The ATLAS detector has an excellent standalone muon spectrometer: muon tracks can be found both in the inner detector and the muon spectrometer. A "combined" muon track consists in matched tracks from both the muon spectrometer and inner detector. We require that a muon, with $p_T \geq 30$ GeV,

- forms a combined track (inner detector and muon spectrometer) with $|\eta| \leq 2.5$,
- has a match $\chi^2 < 100.0$ (5 D.O.F) between the parameters of the inner detector and muon spectrometer tracks.

The muons in the 1 TeV Z' sample have a most probable p_T of about 500 GeV. An efficiency of (95 $\pm$ 0.2)% with a resolution of approximately 5% is found with this selection. The results are consistent with previous studies [17, 18].

The muon identification efficiency as a function of p_T has been determined using two methods. The first method is the 'tag and probe' method, which has been used successfully at the Tevatron. In this method one uses a 'standard candle' as an in situ calibration point. It involves selecting $Z \rightarrow \mu\mu$ events and evaluating the reconstruction efficiency from data on these events. One combined muon is used as the tag while an inner detector track is used as a probe track. One can then study how often the probe muon also has a combined track to get an unbiased measurement of the combined muon reconstruction efficiency. The reconstruction efficiency was measured by fitting to the dimuon invariant mass spectrum and finding the fraction of events where the probe track was found as a combined track. A comparison between this tag and probe method and Monte Carlo truth is shown in Fig. 2. The Monte Carlo truth efficiency is determined by counting the number of generated muons with successfully reconstructed inner detector tracks that also have a combined muon track. This study demonstrates that we should be able to use this method to extrapolate into the very high p_T range.

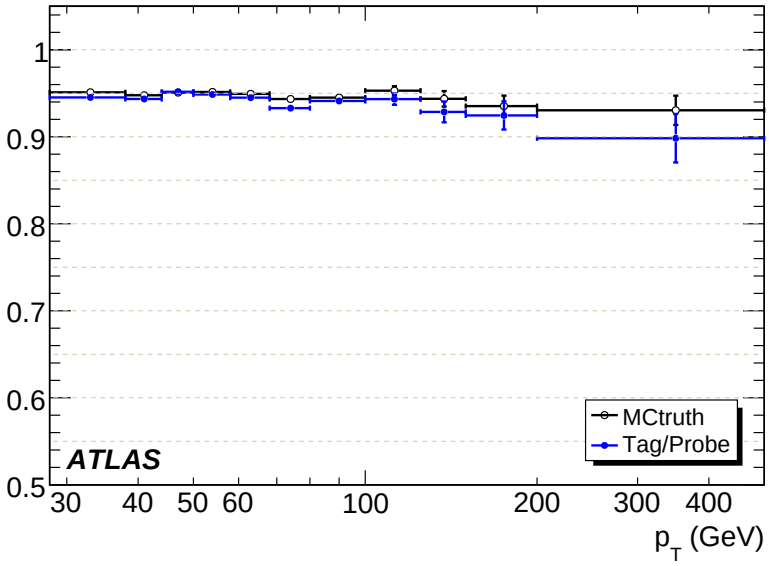

Figure 2: Efficiency of muon reconstruction and identification as a function of p_T from two different methods (see text).

2.3 Tau Identification

The algorithm to reconstruct hadronically decaying τ lepton candidates is described in [19]. It is calorimeter based; it starts from a reconstructed cluster with a transverse energy[4] $E_T > 15$ GeV and then builds identification variables based on information both from the electromagnetic and hadronic calorimeters, as well as the inner tracker. Finally, an electron and a muon veto are applied, which means that hadronically decaying τ candidates which are matched (which "overlap") with an identified electron or muon are removed.

[4] The transverse energy is defined as the energy multiplied by $\sin\theta$, where θ is the angle between the beam axis and the direction from the interaction point to the cluster.

The reconstruction efficiency, defined as the probability of a true hadronically decaying τ to be reconstructed as a cluster, and normalized to all true hadronically decaying τ leptons with E_T >15 GeV inside the η acceptance, is flat as a function of η and ϕ. The average efficiencies are summarized in Table 2. Efficiencies for electron and muon vetoes are given with respect to all reconstructed τ leptons.

Events in $\|\eta\| \leq 2.5$	(87.1 ± 0.1) %
Events in $\|\eta\| \leq 2.5$ AND E_T >15 GeV	(85.6 ± 0.2) %
Reconstruction	(98.8 ± 0.1) %
Electron veto	(99.3 ± 0.1) %
Muon veto	(99.9 ± 0.0) %

Table 2: Reconstruction efficiency, efficiency of e/μ-τ-jet overlap removal for hadronically decaying τ leptons from Z' boson decays. The efficiencies for kinematic requirements are also given.

A likelihood is computed for each τ candidate. The τ likelihood combines information from the calorimeter describing the shower shape and tracking information in a multivariate likelihood to maximize the discrimination from background. Detailed studies were done to optimize the τ lepton efficiency and jet rejection for the Z' boson search. The result (shown in Table 3) was to impose a p_T-dependent likelihood requirement, a requirement on the number of tracks, and a requirement on the transverse energy.

3 Trigger

The aim of the trigger system is to reduce the rate of events flowing through the data acquisition to 200 Hz while maintaining a highly efficient selection for rare signal processes. Even at the initial luminosity of $\mathscr{L} = 10^{31}\ cm^{-2}s^{-1}$, it will be a challenge to keep the trigger highly efficient for all important final states. Several detailed trigger studies were undertaken for the dilepton final state. In this section we summarize those results.

3.1 Electron Triggers

There are several proposed triggers which in principle can be used for the dielectron analysis. We studied four triggers: `e55` - requiring one electron with $p_T \geq 60$ GeV, `e22i` - requiring one isolated electron with $p_T \geq 25$ GeV, `2e12` - requiring two electrons with $p_T \geq 15$ GeV, and `2e12i` - requiring two isolated electrons with $p_T \geq 15$ GeV.

Table 4 shows the efficiency at the three ATLAS trigger levels [20]: level 1 (L1), level 2 (L2), and the event filter (EF) for a sample of graviton events. As can be seen in this table, the most efficient triggers are the high p_T triggers that do not require isolation. The low p_T triggers (`2e12`, `2e12i`) will not be considered any further.

Requirement	Efficiency (%)
$E_T > 60$ GeV	89.8 ± 0.2
AND $1 \leq N_{trk} \leq 3$	79.2 ± 0.3
AND likelihood requirement	51.0 ± 0.3

Table 3: Preselection and identification efficiency for $Z' \rightarrow \tau\tau$ ($m = 600$ GeV). Efficiency is given with respect to reconstructed hadronically decaying τ leptons (after removal of overlap with electrons or muons).

Signature	Efficiency (L1/L2/EF) (%)			Total Trigger Efficiency (%)
e55	99.9 ± 0.0	95.9 ± 0.2	94.6 ± 0.3	90.8 ± 0.3
e22i	85.9 ± 0.3	96.4 ± 0.4	83.9 ± 0.3	80.9 ± 0.4
2e12	99.9 ± 0.1	84.9 ± 0.5	85.5 ± 0.3	72.6 ± 0.6
2e12i	59.1 ± 0.7	86.1 ± 0.7	86.2 ± 0.3	43.9 ± 0.7

Table 4: Trigger level efficiencies on $G \rightarrow e^+e^-$ ($m = 500$GeV) events with respect to *loose* electron offline selection. The last column shows the overall trigger efficiency after all levels.

Sample	mu20 Efficiency (L1/L2/EF) (%)			Total Trigger Efficiency (%)
$m = 400$ GeV ρ_T/ω_T	97.6 ± 0.1	98.8 ± 0.1	99.5 ± 0.1	96.0 ± 0.1
$m = 600$ GeV ρ_T/ω_T	98.1 ± 0.1	98.5 ± 0.1	99.2 ± 0.1	95.9 ± 0.1
$m = 800$ GeV ρ_T/ω_T	97.6 ± 0.1	98.7 ± 0.1	99.2 ± 0.1	95.6 ± 0.1
$m = 1$ TeV ρ_T/ω_T	97.6 ± 0.1	98.7 ± 0.1	99.2 ± 0.1	95.6 ± 0.1
$m = 1$ TeV Z'_χ	97.8 ± 0.1	98.9 ± 0.1	99.5 ± 0.0	96.3 ± 0.1
$m = 2$ TeV Z'_{SSM}	97.6 ± 0.1	98.7 ± 0.1	98.9 ± 0.1	95.3 ± 0.2

Table 5: Simulated trigger level efficiencies of dimuon resonance samples with respect to offline selection. The last column shows the overall trigger efficiency after all levels.

3.2 Muon Triggers

For the dimuon channel we investigated the trigger efficiency for dimuon events using the single muon 20 GeV p_T trigger mu20 [20] . Results for various signal samples are shown in Table 5. Detailed studies on ways to estimate the trigger efficiency were carried out and presented in [21]. It was found that a tag and probe method, similar to the method described for the offline muon reconstruction, could be used to extrapolate $Z \rightarrow \mu\mu$ results to high p_T. In addition, efficiencies were obtained using orthogonal triggers, giving a sample which was minimally biased with respect to the muon triggers. It was found in [21] that these estimates agreed with both the tag and probe method and the results from the simulated samples shown here. As can be seen from Table 5 the single muon triggers are highly efficient for any of our signal samples with a total trigger efficiency around 95%.

3.3 Triggers for Taus

The τ lepton decays to hadronic states in 65% of the cases, and the rest of the time to lighter leptons (e or μ). In our studies of ditau final states we select events triggered with a single lepton (e/μ) trigger. Thus, we consider two true final states, which we denote $e\tau_h$ and $\mu\tau_h$.

For the $e\tau_h$ channel we consider two triggers: e22i and e55, as studied in section 3.1. The $\mu\tau_h$ events are selected using the mu20 trigger already used in section 3.2. Note that the efficiencies shown here are lower than for the dimuon or dielectron channel. This arises because there is only one electron or muon in the final state considered here while in the dielectron or dimuon final state either electron/muon can satisfy trigger requirements. Table 6 summarizes the trigger efficiencies.

4 Standard Model Predictions and Other Sources of Systematic Uncertainties

In this section, we investigate the main background sources and we show the dominance of the neutral Drell-Yan process. Then we investigate the uncertainties in the Standard Model predictions for Drell-Yan

Signature	Efficiency (L1/L2/EF) (%)			Total Trigger Efficiency (%)
`e22i`	85.2 $\pm$0.5	89.8 $\pm$0.4	90.2 $\pm$0.3	69.1 $\pm$0.6
`e55`	90.0 $\pm$0.3	74.2 $\pm$0.4	78.7 $\pm$0.6	52.6 $\pm$0.8
`e22i` or `e55`	96.7 $\pm$0.1	88.7 $\pm$0.4	88.9 $\pm$0.3	75.5 $\pm$0.5
`mu20`	79.8 $\pm$0.6	90.7 $\pm$0.4	97.5 $\pm$0.4	70.6 $\pm$0.5

Table 6: Trigger level efficiencies for different triggers for τ leptons from $m = 600$ GeV Z' bosons decaying to $e\tau_h$ and $\mu\tau_h$ final states with respect to offline selection. The last column shows the overall trigger efficiency after all levels.

production, as well as for an extra neutral gauge boson. Finally, we discuss the experimental sources of uncertainties, including a dedicated study of the effect of the muon spectrometer alignment.

4.1 Background Sources

The neutral Drell-Yan (DY) process constitutes the irreducible background in the search for new heavy dilepton resonances.

The dielectron reducible background results from events in which one or two electrons come from the jet→electron or photon→electron contamination. In addition, true isolated electrons can produced by $W \to e\nu$ or $Z \to ee$ decays. By combining these effects in the dielectron case, one can list the reducible background sources: inclusive jets, W+jets, W+photon, Z+jets, Z+photon, photon+jet and photon+photon. For a first estimation of these backgrounds, we have used the event generator PYTHIA [22] to compute the differential cross-sections as a function of the invariant mass of the object pair. The results are shown on the left of Fig. 3. The neutral Drell-Yan process has a much lower cross-section than most of the backgrounds. For each electron-candidate leg originating from a jet (photon), we then apply a rejection factor[5)] of $\mathrm{R}_{e-jet} = 4 \times 10^3$ ($\mathrm{R}_{e-\gamma} = 10$) [15]. We apply an additional requirement to take into account the geometrical acceptance in which the electrons are identified, i.e. $|\eta| < 2.5$, and require at least one object with $p_T \geq 65$ GeV. The resulting differential cross-sections are shown on the right of Fig. 3. One can see that each contribution represents at most 25% of the neutral Drell-Yan process. The sum of all contributions does not exceed 30%. Both the transverse momentum and the rapidity requirements play an important role in reducing the QCD-jet background because it is produced mainly in the t-channel resulting in jets with high rapidities. Further reduction of these backgrounds may be obtained by requiring opposite electric charges.

The WW, WZ, ZZ and top pair processes can also produce two opposite sign electrons. Whereas the cross-sections of the diboson processes are of the same order as the smallest backgrounds above, the top pair cross-section is not negligible. As the topology of the events is not as simple as in the above backgrounds, no conclusion can be drawn without a full simulation study. Using a sample of fully leptonic and semi-leptonic $t\bar{t}$ events, it was checked that the $t\bar{t}$ background was of the order of 10% of the Drell-Yan contribution for di-object masses above 500 GeV after applying electron identification and the same rejection factor as above to the most energetic jet.

The rejection factors μ-jet and μ-photon are higher than the ones corresponding to the electrons and the resulting reducible backgrounds are lower.

All these assumptions will have to be checked with the real data. One can use for instance electron-muon or same charge samples, in which no signal is expected.

[5)] This number is given for the *medium* selection while the *loose* selection was used here. However, this corresponds to an efficiency of (80.6 ± 0.2)%, which is higher than our average efficiency using *loose* criteria, due to the better performance of the more recent release used in [15].

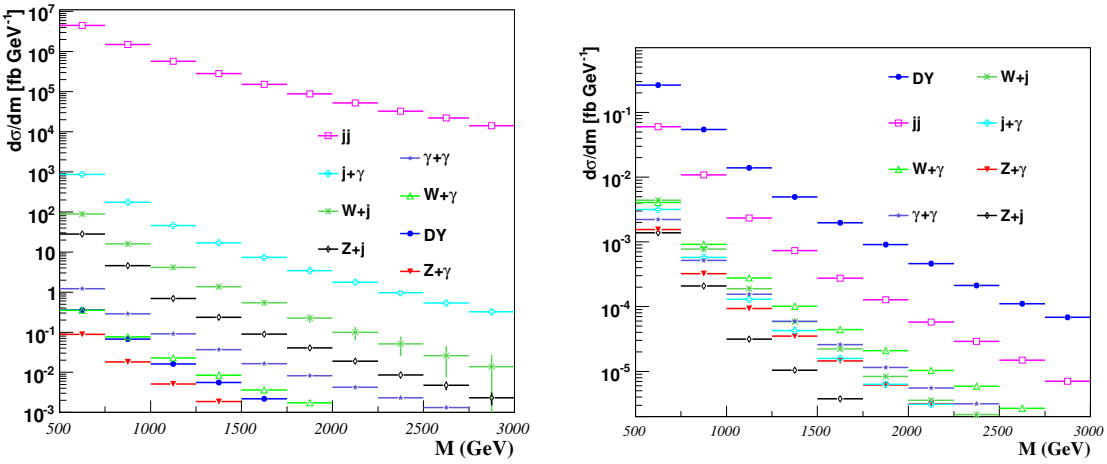

Figure 3: Background contribution to the e^+e^- invariant mass spectrum: before selection requirements (left) and after selection requirements (right).

In the following, only the neutral Drell-Yan is considered as a source of background in the dilepton channel. The ditau case is treated later.

4.2 Controlling the Dilepton Cross-Section

The background estimations in the last section were performed with the PYTHIA event generator which uses tree-level calculations of the cross-sections. The tree-level dilepton cross-sections are subject to large higher order electroweak and QCD corrections. These are known at least to next-to-leading order (NLO) of perturbation theory, not only for the Standard Model Drell-Yan process, but also for a number of new physics processes. They have the additional benefit of reducing the uncertainty induced by the *a priori* unknown renormalization and factorization scales $\mu_{R,F}$. In the following, we discuss in detail the various known radiative corrections and the remaining theoretical uncertainties, focusing on the Standard Model Drell-Yan process and the corrections to the tree-level cross-section.

4.2.1 NLO Electroweak Corrections

The electroweak corrections to the Drell-Yan process are known to NLO in the fine-structure constant α [23, 24]. Initial-state photon radiation must be factorized into the parton density functions (PDFs), which in principle modifies the DGLAP evolution of quarks and gluons, but has in practice little effect on the quality of the global fit [25]. Only at very large x and μ_F^2 can the correction become of the order of 1%. Multiple initial-state photon emission can also be resummed, leading to a 0.3% modification of the cross-section [26], or matched to parton showers [27]. The remaining initial-state QED contributions are also small, whereas the photon radiation emitted by the final state leptons can have a significant impact on their mass (M) and transverse momentum spectra as well as the forward-backward asymmetry A_{FB} [28].

In the vector-boson resonance region(s) these and the universal parts of the weak corrections, which can amount to $+80$ ($+40$) % for muon (electron) pairs below and -18 (-10) % above the resonance, can be taken into account by using a running value of $\alpha(M^2)$ or, more generally, effective vector and axial vector couplings in the Effective Born Approximation. The corrections are then reduced to $+6$

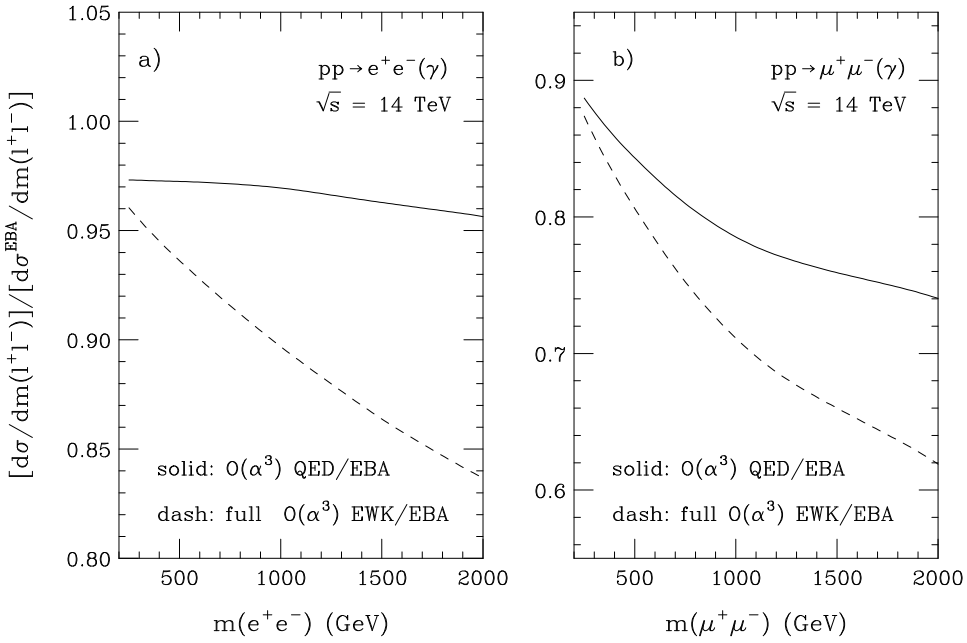

Figure 4: NLO electroweak corrections in the high-mass region for Standard Model electron and muon pair production at the LHC [23]. In the presence of a new resonance, these relative corrections would be largely reduced (see text).

(+2) % for muon (electron) pairs below and +1 (< +1) % above the resonance. While the presence of new physics can modify the running of the weak parameters, the QED corrections remain unaffected.

The electroweak corrections coming from non-factorisable box diagrams with double-boson exchange are small in the Z (and Z') resonance region(s), but they can be quite large away from these resonances (-4 to -16 % for electron pairs, -12 to -38 % for muon pairs of invariant mass 300 GeV to 2 TeV at the LHC, see Fig. 4).

4.2.2 NLO QCD Corrections

The QCD corrections to the Standard Model Drell-Yan process are known at NLO [29] and next-to-next-to-leading order (NNLO) [30, 31] in the strong coupling constant α_s. The latter include in principle non-factorisable corrections through qq and gg initial states, which remain, however, smaller than 1% in practice, even at small values of x, where the gluon density is large. The effects of multiple soft-gluon radiation have been resummed simultaneously in the low-p_T and high-mass (above 500 GeV) regions at next-to-leading logarithmic (NLL) accuracy not only for Standard Model Z-bosons [32], but also for Z' bosons [33]. They were shown to be in good agreement with the NNLO result as well as the one obtained by matching NLO QCD to parton showers in MC@NLO [33, 34]. In contrast, the matching of tree-level matrix elements to parton showers in PYTHIA [22] requires the *ad hoc* application of a (slightly) mass-dependent correction (K) factor and leads to an unsatisfactory description of the p_T spectrum. For resonant spin-2 graviton production, which involves not only color-triplet quark, but also color-octet gluon initial states, the NLO QCD corrections are substantially larger ($K \simeq 1.6$) [35, 36] than those for Standard Model or extra neutral gauge bosons ($K \simeq 1.26$, see Fig. 5). In this case, the matching of matrix elements to parton showers has only been performed at the tree-level [37], and resummation has only been performed in the low-p_T region [36].

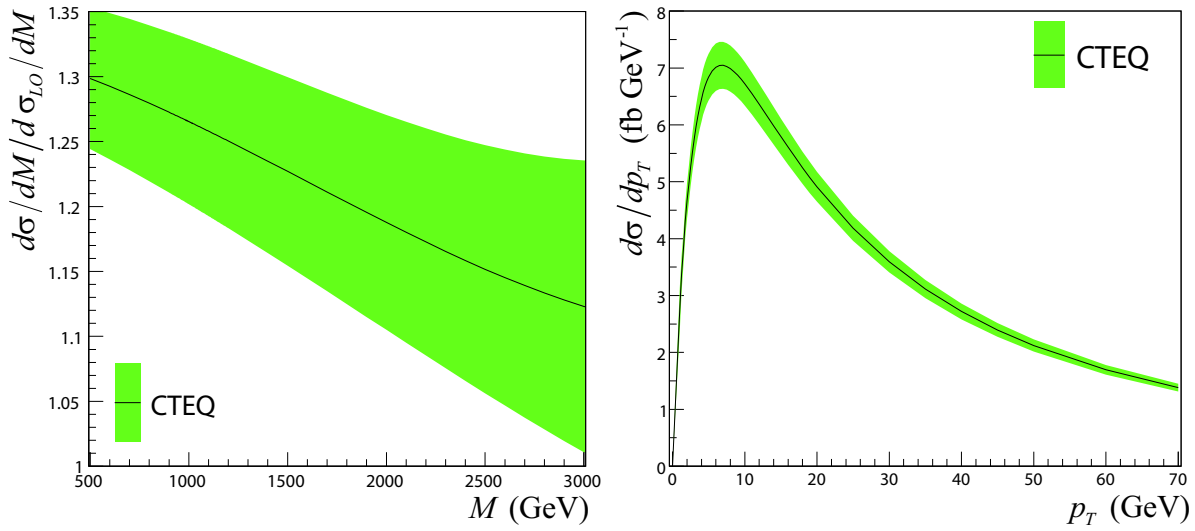

Figure 5: Mass (left) and transverse-momentum (right) spectra after matching the NLO QCD corrections to joint resummation with CTEQ6M parton densities. The mass spectra have been normalized to the LO QCD prediction using CTEQ6L parton densities. The shaded bands indicate the deviations allowed by the up and down variations along the 20 independent directions that span the 90% confidence level of the data sets entering the CTEQ6 global fit.

While the NLO total cross-sections for vector bosons and gravitons still change substantially when the renormalization and factorization scales are varied simultaneously around the resonance mass M by a factor of two ($\pm 9\%$) [33, 36], the scale uncertainty is reduced to the percent-level at NNLO [30, 31] or, alternatively, to $+6$ and -3 % after joint resummation at the NLL order [33].

The theoretical uncertainty coming from different parameterizations of parton densities is estimated in Fig. 5 [33] for invariant masses above 500 GeV. Since the invariant mass of the lepton pair is correlated with the momentum fractions of the partons in the external protons, the normalized mass spectra (left) are indicative of the different shapes of the quark and gluon densities in the CTEQ6M[6)] parameterization [38]. The latter also influence the transverse-momentum spectra (right). The shaded bands show the uncertainty induced by variations, added in quadrature, along the 20 independent directions that span the 90% confidence level of the data sets entering the CTEQ6 global fit [39]. With about $\pm 5\%$ at 1 TeV ($\pm 11\%$ at 3 TeV), the PDF uncertainty is slightly larger than the scale uncertainty [33, 40].

The uncertainty at low transverse momenta coming from non-perturbative effects in the PDFs is usually parameterized with a Gaussian form factor describing the intrinsic transverse momentum of partons in the proton. Three different parameterizations of this form factor have been proposed [41–43]. In all three cases the transverse-momentum distribution is changed by less than $+3$ and -6 % for $p_T > 5$ GeV [33].

Combining the three contributions (from the scales, the PDFs and the non-perturbative form factor), the total theoretical QCD uncertainty is $\pm 8.5\%$ at 1 TeV, $\pm 14\%$ at 3 TeV. It must be noted that these uncertainties are common to the signal (heavy resonance) and background (Standard Model Drell-Yan).

[6)] CTEQ collaboration has recently proposed new sets of PDFs. Using them, both the central values and uncertainties may change by several percents.

4.3 Effect of Muon Spectrometer Misalignment

At large p_T ($\geq$ 100 GeV), an important contribution to the muon momentum resolution is the alignment of the muon spectrometer. In the early data period, the resolution is expected to be dominated by the alignment. The ultimate goal of the alignment system is to determine the position of the chambers in the muon spectrometer to about 40 μm and $\sigma_{rot}(mrad) = 0.5\sigma_{trans}(mm)$.

A detailed study was carried out in order to determine the effect of possible larger uncertainties in the position of the chambers to the Z' search. For the analysis, in addition to the ideal case of no misalignment at all, we have chosen 7 different hypotheses of misalignment: $(40\mu m, 20\mu rad)$, corresponding to the target value of the alignment system, (100 μm, 50 μrad), (200 μm, 100 μrad), (300 μm, 150 μrad), (500 μm, 250 μrad), (700 μm, 350 μrad) and (1000 μm, 500 μrad). In the last two cases, the alignment resolution is of the same order or greater than the track sagitta we want to measure.

As shown in Fig. 6, the dominant effect leading to a wash out of the signal is the resolution loss[7)]. The loss of resolution due to misalignment will deteriorate our ability to determine the charge of the muon. This was also studied as a function of the misalignment and is summarized in Table 7.

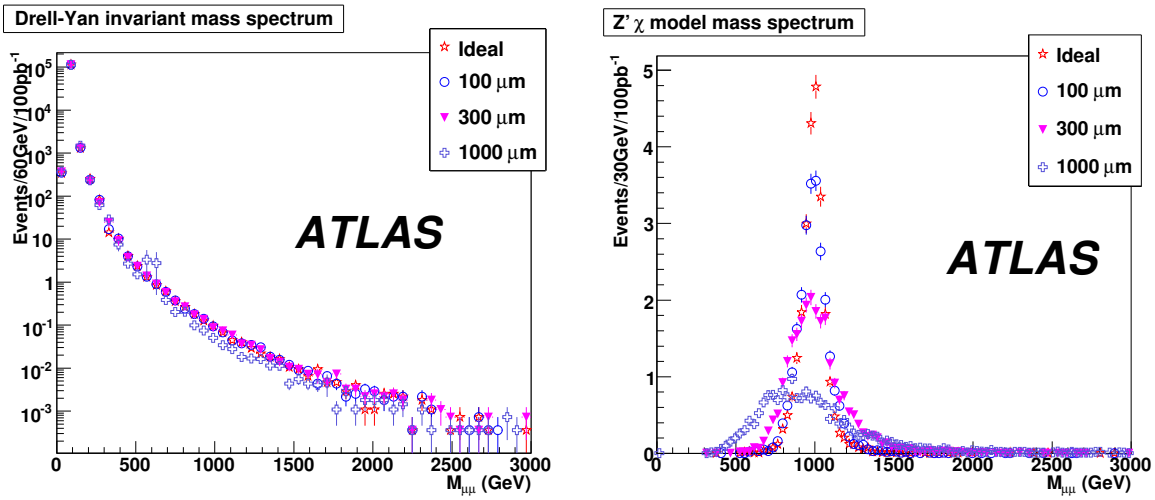

Figure 6: Left: reconstructed invariant mass distribution of Drell-Yan events for different misalignment hypotheses. The numbers corresponds to an integrated luminosity of 100 pb^{-1}. Right: reconstructed invariant mass of the Z'_χ model for the seven misalignment scenarios.

Misalignment (μm)	Ideal	40	100	200	300	500	700	1000
Relative efficiency	0.984	0.984	0.984	0.98	0.973	0.948	0.918	0.877

Table 7: Loss in signal efficiency due to the charge misidentification for seven misalignment hypotheses.

4.4 Other Systematic Uncertainties

Additional experimental systematic uncertainties must be taken into account, listed as follows:

[7)] The slight excess of events around 600 GeV is due to mis-reconstructed Z bosons. In later versions of the software, this effect is not present anymore.

- the uncertainty in the efficiency of object identification was assumed to be 5% for muons, 1% for electrons, and 5% for τ leptons;
- the uncertainty in the energy scale was assumed to be 1% for muons, 1% for electrons, and 5% for τ leptons;
- the uncertainty in the resolution of the objects is as follows: $\sigma(\frac{1}{p_T}) = \frac{0.011}{p_T} \oplus 0.00017$ for muons, 20 % for electrons, and 45% for τ leptons.
- the uncertainty in the luminosity was assumed to be 20% with an integrated luminosity of 100 pb^{-1} of data and 3% for 10 fb^{-1}.

The effect of all the above on the discovery potential is discussed in the next section for individual channels.

5 Search for Exotic Physics

In this section we present the discovery potential for several resonant signatures in the early running of ATLAS. We focus on the reach with an integrated luminosity of up to 10 fb^{-1} of data.

The statistical significance of an expected signal can be evaluated in several ways. The simplest approach, "number counting" is based on the expected rate of events for the signal and background processes. From these rates, and assuming Poisson statistics, one can determine the probability that background fluctuations produce a signal-like result according to some estimator; e.g. the likelihood ratio. In the "shape analysis" approach, a detailed knowledge of the expected spectrum of the signal and background for one observable (like the invariant mass distribution for example) can be used to improve the sensitivity of the search by treating each mass bin as an independent search channel, and combining them accordingly.

The resulting sensitivity is in general higher in the shape analysis than the estimation given in the number counting approach. In the shape analysis, the data is fitted or compared to two models: a background-only model and a signal-plus-background model. These are also called "null hypothesis", noted H0 and "test hypothesis", noted H1, respectively. The input signal and background shapes are given to the fitting algorithms either as histograms in the non-parameterized approach [44] or as functions in the parameterized approach. For each of the models, a likelihood or a χ^2 distribution is computed and the log of the ratio of the two likelihoods (LLR) or the difference of two χ^2s are estimated and used to compute the confidence levels. Either $CL_b = CL_{HO}$ alone, or $CL_s = CL_{H1}/CL_{H0}$ (in the "modified frequentist approach" [44]) can then be used to compute the significance S:

$$S = \sqrt{2} \times Erf^{-1}(1 - CL_b) \quad \text{or} \quad S = \sqrt{2} \times Erf^{-1}(1 - \frac{1}{CL_s}) \tag{1}$$

in the *double tail* convention[8)].

A convenient way to compute the LLR is to use the Fast Fourier Transform (FFT) method presented in [45]. The advantage of this method is that it does not require the generation of millions of pseudo-experiments needed for high significances and which can be time consuming. The sources of systematic uncertainties can then be incorporated as nuisance parameters.

The above methods have been used to investigate the discovery potential of the Z' boson in the dilepton (e, μ, τ) channels, of the graviton in the dielectron channel, and of Technicolor in the dimuon channel. This is presented in the following sections.

[8)] In this convention, $1 - CL_b$ has to be lower than 2.87×10^{-7} to correspond to a 5σ significance.

5.1 Background Estimation

As discussed in the previous section, neutral Drell-Yan production of lepton pairs is expected to be the dominant background for all the analyses (but $\tau^+\tau^-$) and other contribution will be neglected here. Since different techniques are used to estimate the signal significance we also treat the Drell-Yan background in a few different but entirely consistent ways:

- In the "number counting" approach, we simply count the expected number of events under the resonance peak from various background sources, including the Drell-Yan process.
- In the non-parameterized CL_s method, we use the number and shape of the mass distribution by producing a histogram for the background.
- For several analyses, we perform a fit to the Drell-Yan background parameterizing the shape which allows to estimate the number of background events and extrapolate it to higher masses.

Each of these methods produces a complementary and consistent approach to estimating the main background. When the Drell-Yan fit is needed, we parametrize the shape of the background by the formula ae^{-bM^c}, where M is the invariant mass of the lepton pair and a,b,c are parameters of the fit. Fits to the Drell-Yan spectrum presented in section 4.2 suggest that the parameterization $exp(-2.2M^{0.3})$ used by [46] describes the background shape well. It is this one which is used in the $Z' \to \mu\mu$, $G \to ee$ and technicolor analyses. In the $Z' \to ee$ analysis, these parameters are allowed to vary in the individual ensemble tests. The fit to the entire spectrum letting all parameters float is consistent with this prescription.

5.2 $Z' \to ee$ Using a Parameterized Fit Approach

5.2.1 Event Selection

The selection of events with two electrons coming from a Z' has been studied in samples of fully simulated $Z'_\chi \to e^+e^-$ events with Z' boson masses of 1, 2 and 3 TeV, corresponding respectively to integrated luminosities of 21 fb^{-1}, 204 fb^{-1} and 2392 fb^{-1}.

The first requirement is that the two highest p_T clusters in the event be in the geometrical acceptance. The next requirement is that these clusters be associated with a track; its efficiency is 67% at 1 TeV and decreases for higher masses. The third requirement is that these two reconstructed electron candidates be identified as *loose* electrons. The relative efficiency of such a selection is at least 94% and increases with invariant mass. The trigger studies have been normalized to events with two *loose* electrons. As shown in section 3.1, the highest trigger efficiency is obtained with a non-isolated single electron trigger (`e55`). Its efficiency is 90.8% per event. The last requirement is that the two electrons have opposite electric charges. The requirement flow is presented in Table 8, where the events are counted in a window of $\pm 4\ \Gamma_{Z'}$ around the center of the resonance. Although the opposite charge requirement is optional in the absence of a large background, especially at very high invariant mass, it allows to have a control sample (made of same sign dielectrons) for the background. The resulting overall efficiency is 48% at $m = 1$ TeV, 42% at $m = 2$ TeV and about 34% at $m = 3$ TeV.

The above efficiencies, normalized to events in the geometrical acceptance ($|\eta| < 2.5$), are shown in Fig. 7 (left) as a function of the invariant mass of the electrons. They do not depend on the model used to generate the Z' samples. Only the requirement that the two electrons be in the geometrical acceptance depend on the model. Indeed, the relative proportions of initial quark flavors depend on the couplings of the Z' to the quarks. The PDF of the up quarks being harder than that of the down quarks, Z' produced by a $u\bar{u}$ pair tend to be slightly more boosted, and therefore the electrons stemming from their decay tend to be produced at slightly higher pseudo-rapidities. This effect is visible in Fig. 7 (right) showing the efficiency of the $|\eta|$ selection for $u\bar{u}$ and $d\bar{d}$ events separately, and for a number of benchmark Z'

Selection	Signal at 1 TeV	DY at 1 TeV	Signal at 2 TeV	DY at 2 TeV	Signal at 3 TeV	DY at 3 TeV
	347.	3.56	14.7	0.16	1.22	0.015
2 generated $e^{\pm}$, $\|\eta\| < 2.5$	299.	3.07	13.7	0.15	1.16	0.013
2 clusters with a track	201.	2.06	8.0	0.09	0.62	0.009
2 *loose* electrons	190.	1.96	7.2	0.08	0.52	0.008
At least one $p_T > 65$ GeV	190.	1.96	7.2	0.08	0.52	0.008
Event triggered	173.	1.77	6.6	0.07	0.47	0.007
2 opposite charges	166.	1.70	6.2	0.07	0.43	0.007

Table 8: Requirement flow table for the $Z' \to e^+e^-$ analysis: cross-sections in fb. The events are counted in a window of $\pm 4\,\Gamma_{Z'}$ around the resonance.

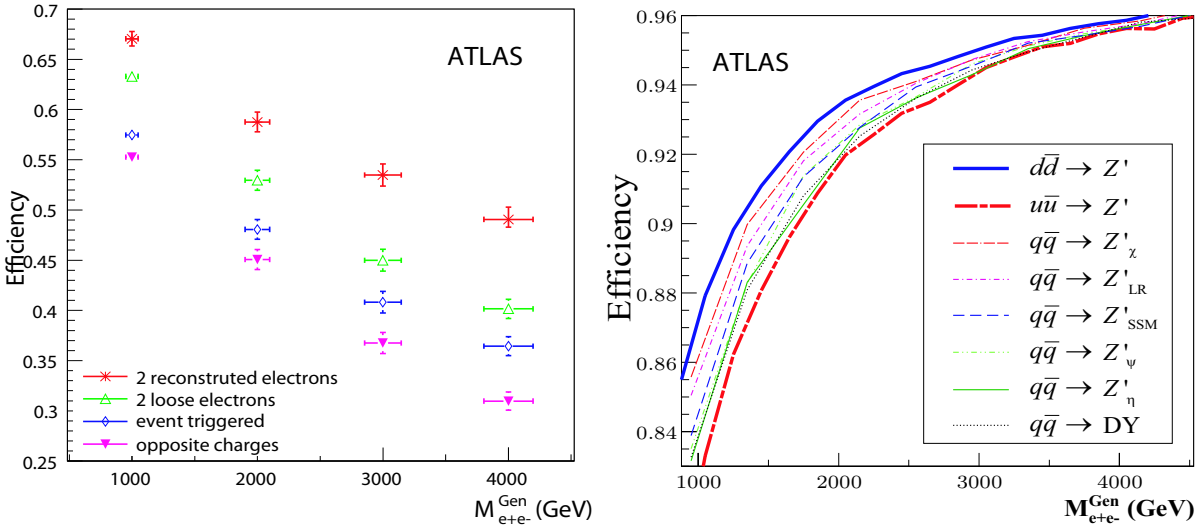

Figure 7: $Z'_\chi \to e^+e^-$ selection efficiency as a function of the generated invariant mass. Left: all selections, normalized to events in the geometrical acceptance; right: $|\eta| < 2.5$ criteria for $u\bar{u}$ and $d\bar{d}$ events separately and for different Z' models (generator level).

models: the Sequential Standard Model (Z'_{SSM}), the E_6 models Z'_ψ, Z'_χ, Z'_η, and the left-right symmetric model (Z'_{LR}). It is therefore possible to generalize the efficiencies that have been measured in the fully simulated samples to models which haven't been simulated as well as to intermediate masses.

5.2.2 Discovery Potential

Modeling of the dilepton invariant mass spectrum. In order to compute the significance for several Z' models, a parameterization of the mass spectrum of the signal and of the background has been used. The differential cross-section can be factorized with a good precision in a parton-level term $\frac{d\hat{\sigma}}{dm}$ and a PDF-dependent term $G_{PDF}(m)$:

$$\frac{d\sigma}{dm}(m) = \frac{d\hat{\sigma}}{dm}(m) \times G_{PDF}(m) \tag{2}$$

Using this factorization, one can write:

$$\left.\frac{d\sigma}{dm}\right|_{\text{DY}}(m) = \frac{1}{m^2} \times G_{PDF}(m) \tag{3}$$

$$\begin{aligned}\left.\frac{d\sigma}{dm}\right|_{\text{Signal}}(m) &= \frac{1}{m^2} \times G_{PDF}(m) \\ &+ \mathscr{A}_{\text{peak}} \times \frac{\Gamma_{Z'}^2}{m_{Z'}^2} \frac{m^2}{(m^2 - m_{Z'}^2)^2 + m_{Z'}^2\Gamma_{Z'}^2} \times G_{PDF}(m) \\ &+ \mathscr{A}_{\text{interf}} \times \frac{\Gamma_{Z'}^2}{m_{Z'}^2} \frac{m^2 - m_{Z'}^2}{(m^2 - m_{Z'}^2)^2 + m_{Z'}^2\Gamma_{Z'}^2} \times G_{PDF}(m)\end{aligned} \tag{4}$$

where $\mathscr{A}_{\text{peak}}$ is the amplitude of the Z' process and $\mathscr{A}_{\text{interf}}$ is the amplitude of the interference Z'/Z and Z'/γ, both normalized to the Drell-Yan process. This parameterization only depends on four parameters: $m_{Z'}$, $\Gamma_{Z'}$, $\mathscr{A}_{\text{peak}}$ and $\mathscr{A}_{\text{interf}}$. The differential cross-section is then multiplied by the appropriate K-factor (see section 4.2). The detector performance is accounted for as follows: the differential cross-section is multiplied by the efficiency computed above and convoluted by the invariant mass resolution (see section 2.1). The agreement between this parameterization and the full simulation is shown in Fig. 8 (left) for a Z'_χ at 1 TeV.

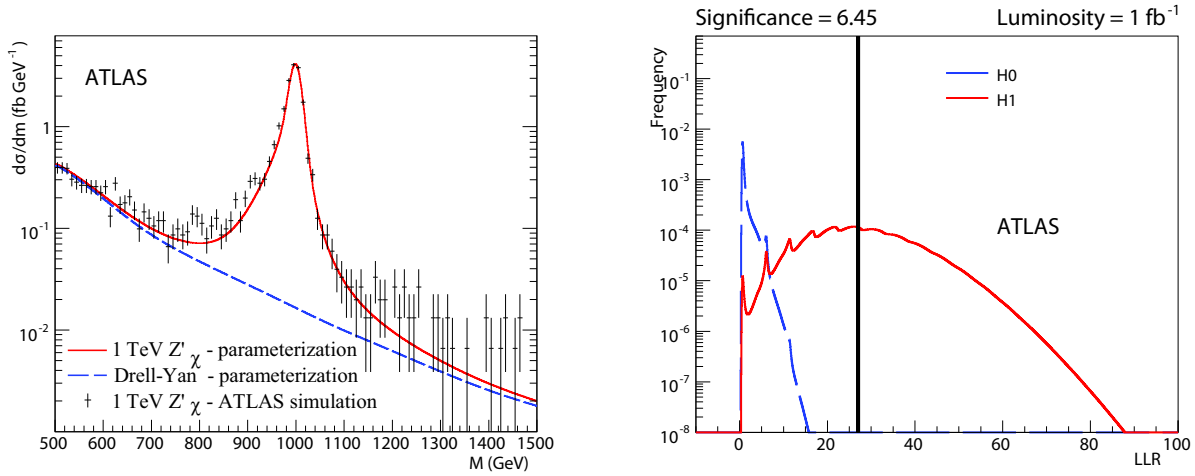

Figure 8: Left: mass spectrum for a $m = 1$ TeV $Z'_\chi \to e^+e^-$ obtained with ATLAS full simulation (histogram) and the parameterization (solid line). The dashed line corresponds to the parameterization of the Drell-Yan process (irreducible background). Right: Log-likelihood ratio densities with 1 fb^{-1} for a $m = 2$ TeV Z'_χ for the signal and background hypotheses. The vertical line is the median experiment in the H1 hypothesis.

Results Using the parameterization presented above to generate mass spectra for signal ($\gamma/Z/Z' \to e^+e^-$) and background ($\gamma/Z \to e^+e^-$), one can compute the distributions of the log-likelihood ratio of the signal (H1) and background (H0) hypotheses.
Figure 8 (right) shows the LLR distributions obtained for a 2 TeV Z'_χ with 1 fb^{-1} as well as the median signal experiment used to calculate CL_s. The FFT method [45] was used in the computation of the LLR distributions. It is important to note that the mass window used to perform the analysis does not affect the result.

Figure 9 (left) shows the integrated luminosity needed for a 5σ discovery of the usual benchmark Z' models as a function of the Z' mass. Only statistical uncertainties were taken into account. The systematic uncertainties are discussed in the next paragraph. A fixed mass window of $[500\ \text{GeV} - 4\ \text{TeV}]$ was used to compute the significance. Roughly speaking, less than 100 pb^{-1} are needed to discover a 1 TeV Z', about 1 fb^{-1} are needed to discover a 2 TeV Z', and about 10 fb^{-1} are needed to discover a 3 TeV Z'.

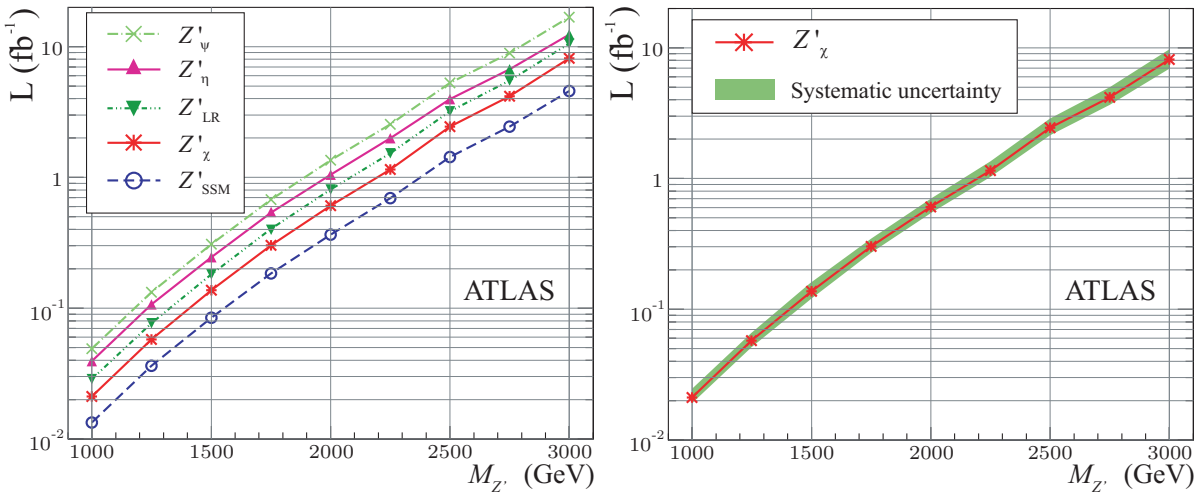

Figure 9: Integrated luminosity needed for a 5σ discovery of $Z' \to e^+e^-$ as a function of the Z' mass. Left: for various benchmark models with statistical uncertainties only; right: for the Z'_χ with systematic uncertainties included.

Systematic Uncertainties The sources of systematic uncertainties were listed in section 4. Since the main background is the Drell-Yan process, the systematic uncertainties from both the efficiencies and the theoretical predictions on the cross-section will affect the number of signal and background events in the same way, and can be added in quadrature. The uncertainties in the event selection efficiency mainly come from the electron identification and the geometrical acceptance. The former amounts to $2 \times \pm 1\% = \pm 2\%$ for two electrons. Taking the extreme efficiencies for pure $u\bar{u}$ and $d\bar{d}$ events as a conservative estimate, the latter goes from ± 3 to $\pm 0.5\%$. Overall, this represents a systematic uncertainty of $\pm 3.6\%$ to $\pm 0.6\%$ from the event selection. This is small as compared to the theoretical uncertainties, which range from $\pm 8.5\%$ to $\pm 14\%$. The effect of these combined uncertainties on the luminosity needed to discover 1, 2 and 3 TeV Z's is $^{+9}_{-10}\%$, $^{+14}_{-10}\%$, $^{+15}_{-13}\%$ (respectively).

The uncertainty in backgrounds other than the Drell-Yan process is another type of uncertainty. However, given that the Drell-Yan contribution is at the level of about 1% of the signal, any variation of the level of non-Drell-Yan background, which is more than ten times smaller, is negligible.

The uncertainty in the electron energy resolution is another type of uncertainty. In addition to the expected uncertainties in the energy resolution as measured in the calorimeter (see section 4), we have conservatively assumed that there was no increase in precision on the measured dielectron invariant mass coming from the angle measurement provided by the tracker. In this case, the resolution of invariant mass increases from about 1% (see section 2.1) to about 1.5%. The effect of these uncertainties on the luminosity needed for a discovery is $^{+5}_{-2}\%$, independent of the Z$'$ mass.

The last type of uncertainty which has been considered is the electron energy scale. When varied within the expected uncertainties, the discovery luminosity varies by $^{+2.5}_{-0}\%$, independent of the Z$'$ mass.

Combining all the above systematic uncertainties, the luminosity needed to discover, for example, a Z'_χ is shown in Fig. 9 (right). It must be noted that the systematic effect coming from the fact that we do not know a priori the mass of the signal was not taken into account. This is adressed separately in appendix A.

5.3 $Z' \to \mu\mu$ Using a Parameterized Fit Approach

The dimuon channel represents an important complement to the dielectron channel. Although the resolution is expected to be up to an order of magnitude worse in the kinematic regime of interest, reducible backgrounds are expected to be considerably lower as discussed in Section 4.1. This feature makes the dimuon channel competitive, especially with early data where the design background rejection may not be achieved. In this section we consider two signal models decaying into dimuons - the Z'_{SSM} and the Z'_χ boson.

5.3.1 Event Selection

To select events from the $Z' \to \mu\mu$ process we require two muons of opposite charge. The muons are required to fulfill the muon identification criteria studied in Section 2.2, including $p_T \geq 30$ GeV and $|\eta| \leq 2.5$. Events are triggered using the `mu20` trigger described in Section 3.2. As seen in Section 4.1, this should select a sample which consists mainly of $Z/\gamma \to \mu\mu$ with limited contamination from other sources of the order of a few percent. Table 9 indicates the effects of the various requirements on both the signal and background samples.

Sample	Z'_{SSM} (1 TeV)	Z'_χ (1 TeV)	Drell-Yan
Generated	508.6	380.6	13.5
$\|\eta\| \leq 2.5$	366.8	271.5	10.8
$p_T \geq 30$ GeV	364.0	270.1	10.7
Muon identification	342.3	256.0	10.0
Trigger	325.2	243.2	9.5
Opposite charge	324.8	243.0	9.5

Table 9: Selection requirement flow for the $Z' \to \mu\mu$ analysis - cross-sections in fb. Events are counted in a mass window of ± 50 GeV of the resonance mass (signal) and for $m_{\mu\mu} > 800$ GeV (background).

5.3.2 Discovery Potential

To evaluate the discovery potential, we use the FFT method [45], as in section 5.2. The amount of data required to discover a Z' boson is computed from the log-likelihood ratio (LLR) of the signal (H1) and background (H0) hypotheses. Figure 10 shows the $1 - CL_b$ obtained as a function of the integrated luminosity for the two studied Z' boson models at $m = 1$ TeV. The largest expected systematic uncertainty (from misalignment of the muon spectrometer) is shown separately. One can see that the amount of luminosity needed for a 5σ discovery ranges from 20 to 40 pb^{-1}, which is competitive with the dielectron channel.

Systematic Uncertainties Section 4 describes the systematic uncertainties that were considered. As can be seen from Fig. 10 the effect of the nominal systematic uncertainties is modest in this channel.

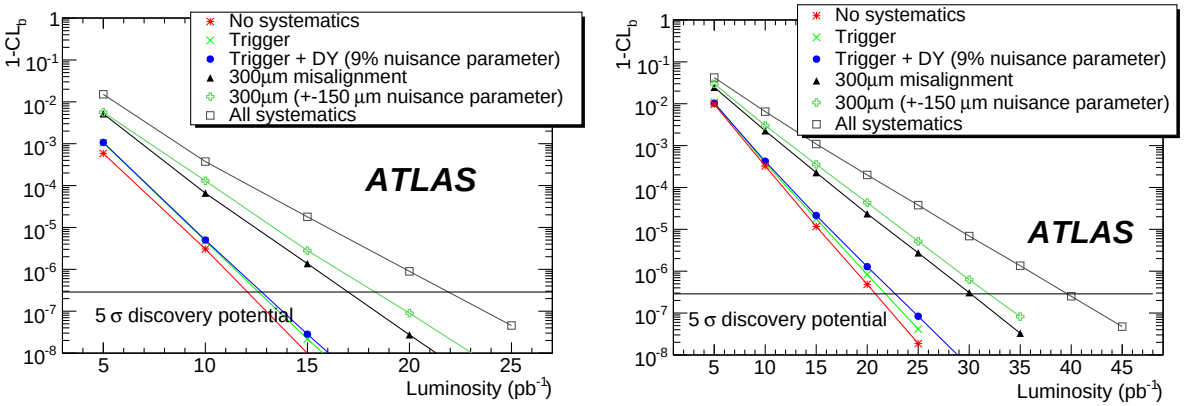

Figure 10: Results of the FFT computation of $1-CL_b$ for $m = 1$ TeV Z'_{SSM} (left) and Z'_{χ} (right) bosons. The horizontal line indicates the $1-CL_b$ value corresponding to 5σ.

The largest theoretical uncertainty entering this study is the knowledge of the Standard Model Drell-Yan cross-section. In the dimuon channel, the largest experimental uncertainty is the resolution for high p_T muons which will be initially dominated by the alignment of the muon spectrometer. As already discussed, the nominal alignment precision may not be achievable with the integrated luminosities presented here and hence could significantly alter the conclusions. Figure 10 shows that the integrated luminosity needed to reach 5σ increases from 13 to 20 pb^{-1} if the muon spectrometer is aligned with a precision of 300 μm. This takes into account an uncertainty of 150 μm on the alignment precision estimate, which will have to be measured in data (e.g. from the $Z \to \mu\mu$ sample) and which is treated as a nuisance parameter in the sensitivity computation.

5.4 $Z' \to \tau\tau$ Using a Number Counting Approach

The ditau signature is an important component to the high mass resonance search. In particular, there are models in which a hypothetical new resonance couples preferentially to the third generation [47]. For these models the branching ratios are such that the dielectron and dimuon channels are not viable - hence it is critical that we consider all possible channels including ditaus. In this section we discuss the discovery potential for such a resonance. Because of finite resources we restrict ourselves to the process $Z' \to \tau\tau$ with a single mass point $m = 600$ GeV although much of the discussion generalizes to a generic ditau resonance search. The ditau final state can be divided into three final states: hadron-hadron (where both τ leptons decay hadronically), hadron-lepton (where one τ lepton decays hadronically and one decays leptonically), and lepton-lepton (where both decay leptonically). Here we consider the hadron-lepton ($h-\ell$) final state. The possibility of observing the hadron-hadron final state using a hadronic τ trigger will be examined later.

5.4.1 Event Selection

To select events in the hadron-lepton final state, we select events with a "hadronic τ" candidate, a charged lepton (muon or electron), and missing transverse energy [9] ($\not\!\!E_T$). As opposed to the dielectron or dimuon channel, the backgrounds to the ditau channel are considerably larger and include Drell-Yan production,

[9] The missing transverse energy was reconstructed using the cell based algorithm described in [48].

W+jets, $t\bar{t}$ and dijet events. After the initial object selection several additional requirements are needed to maximize the expected signal significance.

We consider hadronic τ candidates with $p_T > 60$ GeV and impose a requirement on the likelihood as a function the τ transverse energy as described in Section 2.3. Candidates which overlap with an electron or muon are removed.

For electron candidates we require *medium* electron selection criteria in this analysis (see Section 2.1). The initial muon selection is the same as described in Section 2.2. Since this channel only requires one high p_T lepton the backgrounds are considerably higher than for the dielectron or dimuon final states. To address this we impose additional requirements on the isolation of the lepton. The isolation requirement imposed on electron candidates is $\sum E_{T_{EM}}^{\Delta R<0.2}/p_T < 0.1$ where $\sum E_{T_{EM}}^{\Delta R<0.2}$ is the sum of the energy deposits in the electromagnetic calorimeter within a cone of $\Delta R = 0.2$ from the location in η-ϕ of the electron, less the electron candidate energy. Isolated electrons are required to have $p_T > 27$ GeV. We impose an isolation requirement similar to that of electrons on muon candidates: $\sum E_{T_{EM}}^{\Delta R<0.2} < 0.1$. For isolated muons we require that the χ^2 lie between 0 and 20 and to be considered by the analysis muons must have $p_T > 22$ GeV.

After making the τ candidate selection we make several further requirements to maximize the signal significance. First, we require that $\not{E}_T \geq 30$ GeV. To greatly help with the rejection of the $t\bar{t}$ backgrounds we employ a requirement on the total event p_T which is defined as the sum of $\not{E}_T$ and the vector sum of the hadronic τ with the lepton transverse momentum. We require $p_T^{tot} < 70$ GeV.

The transverse mass of the event is determined by using the lepton kinematics and the event $\not{E}_T$. Defining a four-vector for the missing energy: $\underline{\not{p}_T} = (\not{E}_{T_x}, \not{E}_{T_y}, 0, |\not{E}_T|)$, the transverse mass is calculated as:

$$m_T = \sqrt{2 p_{T,\ell} \not{p}_T (1 - \cos\Delta\phi_{\ell,\not{p}_T})}.$$

We require that $m_T < 35$ GeV.

In the case of the lepton-hadron channel one cannot simply reconstruct the invariant mass of the resonance as energy is taken away from the event by the neutrinos. However, two quantities can be constructed

- A visible mass variable is calculated as defined by CDF [49] using the hadronic τ and the lepton four-vector information:
$$m_{vis} = \sqrt{(\underline{p_\ell} + \underline{p_h} + \underline{\not{p}_T})^2}$$
- The collinear approximation is used to build up the event-by-event invariant mass. The fraction of the τ momentum carried by the visible decay daughters, x_ℓ and x_h, are calculated with the following formulas:
$$x_\ell = \frac{p_{x,\ell} p_{y,h} - p_{x,h} p_{y,\ell}}{p_{y,h} p_{x,\ell} + p_{y,h} \not{p}_x - p_{x,h} p_{y,\ell} - p_{x,h} \not{p}_y}, \; x_h = \frac{p_{x,\ell} p_{y,h} - p_{x,h} p_{y,\ell}}{p_{y,h} p_{x,\ell} + p_{x,\ell} \not{p}_y - p_{x,h} p_{y,\ell} - p_{y,\ell} \not{p}_x}.$$
The reconstructed mass is then calculated as $m_{\tau\tau} = \frac{m_{\ell,h}}{\sqrt{x_\ell x_h}}$.

To greatly help the background rejection and to restrict our search to the region of interest we require $m_{vis} > 300$ GeV. Since the collinear approximation breaks down when the two τ leptons are back-to-back, we impose the requirement that $\cos\Delta\phi_{\ell h} > -0.99$. Of course, since a very heavy particle tends to be produced at rest, the decay objects are mostly back-to-back, leading to a highly inefficient mass reconstruction.

Selection	Signal	$t\bar{t}$	Drell-Yan	Multijet	W+jet
Trigger	1356.	213600.	$2.3950\ 10^7$	$4.19000\ 10^6$	$6.69400\ 10^6$
Lepton	905.	150900.	$1.2600\ 10^7$	$1.08230\ 10^6$	120400.
τ selection	368.	7818.	145680	40080	4587.
Opposite charge	315.	2498.	5306	23240	771.
$\not{E}_T$>30 GeV	270.	2040.	2562	835	162.
$m_T < 35$ GeV	203.2	302.4	388.0	436.4	83.8
$p_T^{tot} < 70$ GeV	155.0	106.7	331.5	221.6	28.4
$m_{vis} > 300$ GeV	132.5	26.2	105.6	33.8	15.0
$\cos\Delta\phi_{\ell h} > -0.99$	13.3	2.1	5.5	2.3	2.7

Table 10: Requirement flow table for the $m = 600$ GeV $Z'_{SSM} \to \tau\tau \to \ell h$ analysis - cross-sections given in fb. The Drell-Yan process includes all flavors of leptons (e^+e^-, $\mu^+\mu^-$, $\tau^+\tau^-$) with an invariant mass of at least 60 GeV.

5.4.2 Discovery Potential for 1 fb^{-1} of Data

Table 10 shows the effect of the various selection requirements for the signal as well as all background processes considered. Distributions of the visible and reconstructed masses for signal and background are shown in Fig. 11. Here we assume a 600 GeV Z' and the SSM cross-section. In 1 fb^{-1} of ATLAS data we estimate 132. signal events and 181. background events after imposing the event selection up to the requirement on visible mass. Using $S/\sqrt{B}$ we estimate the signal significance to be 9.9. The collinear approximation breaks down when the two τ leptons are back-to-back, so that even a loose requirement (such as $\cos\Delta\phi_{\ell h} > -0.99$) reduces the signal by a large factor. Hence, we expect that the search will proceed by looking at the visible mass. If a significant excess over background is seen, the collinear approximation will then be used to help establish the presence of a new resonance.

Systematic uncertainties The systematic uncertainties that were considered are described in Section 4. For an analysis of 1 fb^{-1} of data the dominant systematic source on the signal, just over $\pm$18%, comes from the uncertainty in the luminosity. The second most dominant systematic, the hadronic τ energy scale, affects the signal at the $\pm$10% level. Summing in quadrature the effect of all systematic uncertainties on the signal Monte Carlo sample results in a total systematic uncertainty of about $\pm$20%. The current Monte Carlo samples available for the backgrounds to the ditau analysis are statistically limited and hence prevent a rigorous evaluation of the systematics at this time. As a conservative estimate, we assume that the total systematic uncertainty in the backgrounds is identical to that observed in the signal Monte Carlo. This is a conservative estimate because the majority of the backgrounds in the data have very large cross-sections (dijets, W+jets, etc.) and in principle the evaluation of systematic uncertainties there should be less sensitive to statistical fluctuations than for the signal events. Summing these systematic uncertainties in quadrature and using the formula $S/\sqrt{B+\delta B^2}$ gives a significance of 3.4 in 1 fb^{-1}.

5.5 $G \to e^+e^-$ in a Parameterized Fit Approach

In this section we present a sensitivity study for the Randall-Sundrum $G \to ee$ final state. In this channel, it is assumed that there is no interference between the G and the dilepton background. Table 11 shows the parameters of the different G samples used in this analysis. Γ_G is the simulated graviton resonance width and σ_m stands for the width of the observed resonance after convolution with detector resolutions. For $k/\bar{M}_{pl} < 0.06$ the resonance is narrow compared to the experimental resolution.

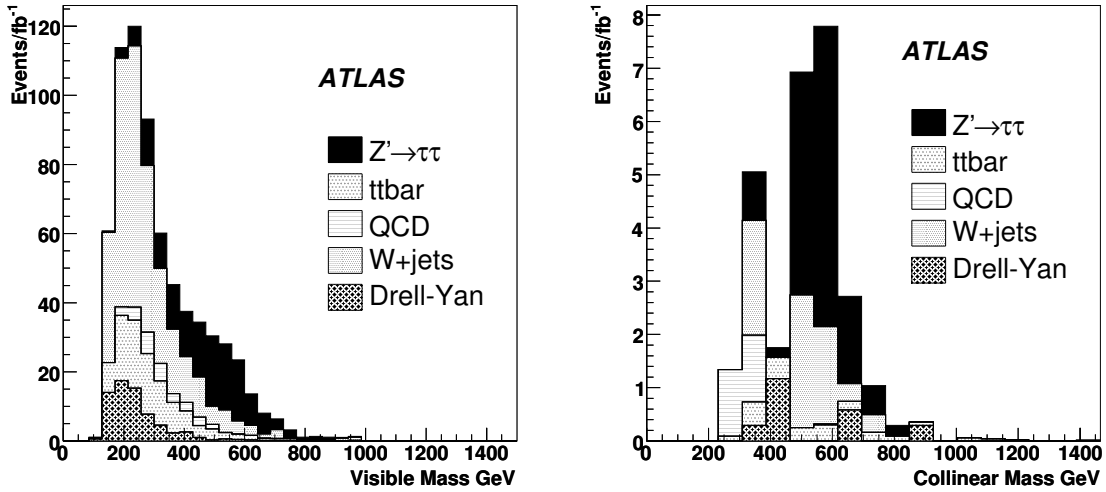

Figure 11: Left: the visible mass distribution in the $Z' \to \tau\tau \to \ell h$ analysis for signal and background processes (1 fb^{-1} of data is assumed). Right: the reconstructed invariant mass obtained using the collinear approximation.

The main Standard Model background is neutral Drell-Yan production. Other backgrounds such as dijets with both jets misidentified as electrons are expected to be small and neglected at this time.

Model Parameters		Γ_G	σ_m	$\sigma \cdot BR(G \to e^+e^-)$
m_G	$k/\bar{M}_{pl}$	[GeV]	[GeV]	[fb]
500 GeV	0.01	0.08	4.6	187.4
750 GeV	0.01	0.10	6.4	27.7
1.0 TeV	0.02	0.57	7.9	26.0
1.2 TeV	0.03	1.62	10.3	22.4
1.3 TeV	0.04	2.98	11.4	25.3
1.4 TeV	0.05	5.02	13.1	26.8

Table 11: Parameters of the $G \to ee$ samples used: natural width (Γ_G), Gaussian width after detector effects (σ_m) and leading order cross-section.

5.5.1 Event Selection

In reconstructing the resonance mass, we require a pair of electrons – we do not make any charge requirements – with $p_T \geq 65$ GeV using the *loose* electron selection criteria described in Section 2.1. We require that the events pass the `e55` single electron trigger (see section 3.1). Finally we require that the two electrons are roughly back-to-back in ϕ with $\cos\Delta\phi_{ee} < 0$ between the two electrons. Table 12 shows the remaining cross-section at each stage of the selection and the total eficiency for different mass points. The efficiency decreases at high graviton masses, due to the track match requirement, which is

consistent with the Z' boson analysis (see section 5.2). Table 13 shows the same requirement flow for the Drell-Yan.

Selection / Sample	500 GeV	750 GeV	1.0 TeV	1.2 TeV	1.3 TeV	1.4 TeV
Generated	187.4	27.7	26.0	22.4	25.3	26.8
Acceptance	172.4	25.9	24.7	21.2	24.0	25.4
Trigger	168.7	25.0	22.6	19.1	21.4	22.3
Electron Id.	127.9	18.3	16.4	12.8	14.6	14.7
$p_T \geq 65$ GeV	125.7	18.2	16.3	12.7	14.5	14.6
$\cos\Delta\phi_{ee} < 0$	123.0	17.8	16.0	12.6	14.3	14.4
Selection efficiency (%)	65.6 ± 1.1	64.4 ± 1.1	61.7 ± 1.1	56.3 ± 1.1	56.4 ± 1.1	53.9 ± 1.1

Table 12: Requirement flow for the $G \rightarrow ee$ analysis. The remaining cross-section (in fb) is given at each stage. The mass window is chosen as $\pm 4\sigma_m$ around the signal peak.

Selection/Sample	500 GeV	750 GeV	1.0 TeV	1.2 TeV	1.3 TeV	1.4 TeV
Generated	20.33	4.91	1.43	0.90	0.51	0.51
Acceptance	18.53	4.50	1.36	0.87	0.48	0.49
Trigger	18.45	4.25	1.16	0.80	0.45	0.44
Electron Id.	14.13	3.18	0.88	0.58	0.38	0.33
$p_T \geq 65$ GeV	13.85	3.15	0.88	0.57	0.38	0.33
$cos\Delta\phi_{ee} < 0$	13.41	3.09	0.85	0.56	0.36	0.33

Table 13: Remaining Drell-Yan cross-section (in fb) at each stage of the $G \rightarrow ee$ analysis. The mass window is chosen as $\pm 4\sigma_m$ around the signal peak.

The Drell-Yan background distribution after this event selection is shown in Fig. 12 along with signal at $m_G = 1$ TeV and coupling $k/\bar{M}_{pl} = 0.02$. The exponential described in Section 5.1 has been used to model the shape of the background.

5.5.2 Discovery Potential

We search for an excess of events in the mass range from 300 GeV up to 2 TeV and study the signal sensitivity by use of "extended maximum likelihood" fitting. We consider two hypotheses. The null hypothesis, H0, is the hypothesis that the data are described by the Standard Model. The test hypothesis, H1, is that the data are described by the sum of the background and a narrow Gaussian resonance.

To investigate the potential for discovery pseudo-experiments are generated from both the null and test hypothesis. Each pseudo-experiment is fit twice. The first fit assumes the data are described by the Standard Model using the function described in Section 5.1. The second fit assumes the data are

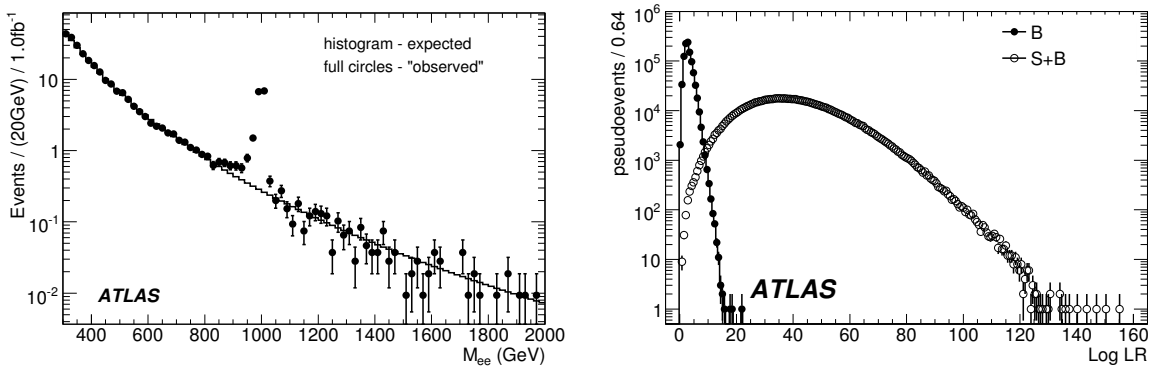

Figure 12: Left: expected (histogram) and "observed" (filled circles) Drell-Yan spectrum from full simulation. The observed distribution includes a graviton with mass of 1 TeV and coupling $k/\bar{M}_{pl} = 0.02$. Note that for the purposes of this plot the vertical axis has been rescaled: the error bars correspond to an integrated luminosity of 100 fb^{-1}. Right: Log likelihood ratio curves for one million pseudo-experiments generated with background only (filled circles), and signal plus background (empty circles) for the same $m = 1$ TeV signal point.

described by the sum of a Gaussian and the shape describing the Drell-Yan background. During this second fit the mean of the Gaussian is allowed to float throughout the entire mass region considered, and the width is fixed to the detector resolution.

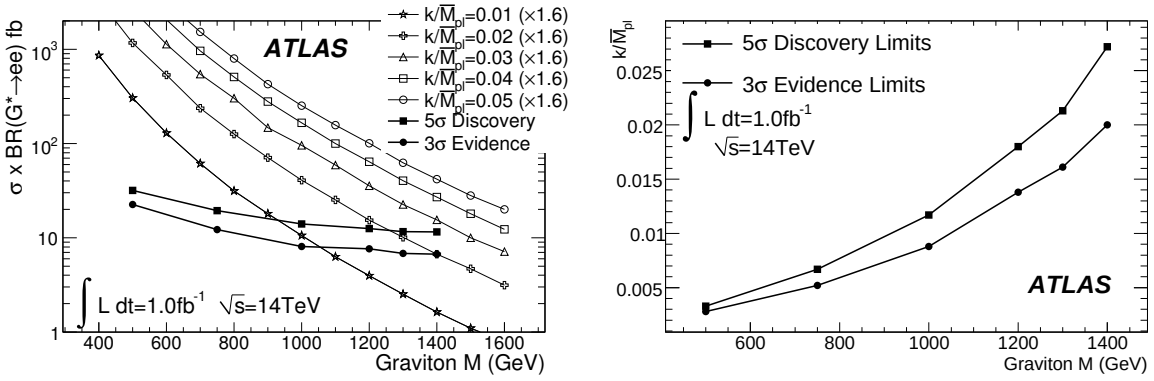

Figure 13: 5σ discovery potential (full squares) as a function of the graviton mass. The 3σ evidence potential is also shown (full circles). Left: shown with cross-sections as calculated by PYTHIA (LO) and multiplied by a K factor of 1.6 for several values of the coupling; right: dependence of the discovery potential on the coupling.

We can then compare the likelihood of the signal and background hypotheses. The distribution of the logarithm of the likelihood ratio between H0 and H1 is constructed, and shown for one signal point in Fig. 12. Based on this, we calculate the average expected discovery potential from the fraction of the likelihood ratio distribution for background-only pseudo-experiments that extends beyond the mean of the distribution for signal plus background experiments. Figure 13 shows the 5σ discovery and 3σ

evidence reach in cross-section and $k/\bar{M}_{pl}$ coupling constant as a function of graviton mass, estimated for an integrated luminosity of 1 fb^{-1}.

The LO cross-sections are multiplied by the *K*-factors discussed in section 4.2.2 for both signal and Drell-Yan background. Various sources of systematic uncertainties for signal and background are considered in the evaluation of the experimental sensitivity, including luminosity, energy scale, energy resolution, electron identification efficiency and Drell-Yan background uncertainties as listed in section 4.4. The combined effect of the systematic uncertainties is to increase the amount of integrated luminosity needed for discovery between 10 and 15 percent for the different parameter sets.

5.6 Technicolor Using a Non-Parameterized Approach

Topcolor-assisted Technicolor models with walking gauge coupling predict new technihadron states that would be copiously produced at the LHC. The lowest mass states are the scalar technipions ($\pi_T^{\pm,0}$) and the vector technirho and techniomega ($\rho_T^{\pm,0}$ and ω_T^0). The vector mesons decay into a gauge boson plus technipion ($\gamma\pi_T$, $W\pi_T$ or $Z\pi_T$,) and fermion-antifermion pairs. This analysis searches for the decays $\rho_T \to \mu^+\mu^-$ and $\omega_T \to \mu^+\mu^-$. The dimuon mode has a lower branching fraction than the modes involving technipions but the signal is clean, straightforward to trigger on, and can be readily observed with early ATLAS data.

The particular model studied here is the "Technicolor Strawman Model" or TCSM [12, 13]. In the TCSM, it is expected that techni-isospin is an approximate good symmetry and therefore the isotriplet ρ_T and isosinglet ω_T will be nearly degenerate. We will assume for what follows that $m_{\rho_T} = m_{\omega_T}$. The technipions are also expected to be nearly degenerate. In the TCSM, the technipion masses are generically not small. In particular, if $m_{\pi_T} > m_{\rho_T}/2$ the decays of the ρ_T and ω_T to technipions would be kinematically forbidden [50]. The dimuon rate is expected to come dominantly from the ω_T with a smaller contribution from the ρ_T.

The event selection is summarized in Table 14. The technivector meson natural widths are less than a GeV, so the observed width $\sigma(m)$ is entirely due to detector resolution.

In principle, the best search sensitivity is not obtained by examining the entire dimuon mass distribution for a bump all at once but by using an optimized mass window that maximizes the signal significance for a given assumed signal mass. A prescription for the optimal window size is taken from an analytic calculation in Ref. [51]. Assuming a narrow Gaussian peak on a linear background, the optimal window was found to be $\pm 1.4\sigma$ about the peak mass. Since we are not really in the narrow resonance regime, we did a study using full-simulation ATLAS Monte Carlo for a Technicolor signal on a Drell-Yan background. Taking $S/\sqrt{B}$ as our measure of significance, Fig. 14 (left) shows that a window size of $\pm \sim 1.5\sigma$ or a bit larger is optimal. For this study, a window size of $\pm 1.5\sigma$ about the peak mass is used.

Figure 14 (right) shows the integrated luminosity necessary to observe either 3σ evidence or a 5σ discovery, using the modified frequentist approach [44], of technimesons in this channel. The systematic uncertainties summarized in section 4.4 were included in this calculation of technimeson search sensitivity. It should be noted that the integrated luminosity needed for 5σ discovery will be affected by the level of misalignment of the muon spectrometer. The contours in Fig. 14 were computed assuming the level of alignment we expect to achieve. The studies in sections 4.3 and 5.3 show that for an initial precision of 300 μm with an uncertainty of 150 μm the amount of data needed to reach 5σ would increase by approximately 50%.

m_{ρ_T,ω_T} (GeV)	400	600	800	1000
Peak mass (GeV)	403	603	804	1004
$\sigma(m)$ (GeV)	13	22	34	46
Requirement				
Generated	201	60.8	23.0	10.1
$\lvert\eta\rvert < 2.5$	116	39.8	15.8	7.3
$p_T > 30$ GeV	114	39.5	15.7	7.2
L1_MU20	112	38.7	15.3	7.0
L2_mu20	110	38.0	15.1	6.9
EF_mu20	109	37.5	14.9	6.8
Match $\chi^2 < 100$	104	35.7	14.0	6.4
Opposite charge	104	35.7	14.0	6.4
Mass window	78.2	26.3	10.3	4.7
Drell-Yan background	46.9	14.1	6.1	2.8
Selection efficiency (%)	38.9 ± 0.5	43.2 ± 0.5	44.8 ± 0.5	46.8 ± 0.5

Table 14: Selection requirement flow for the analysis - cross-section in fb.

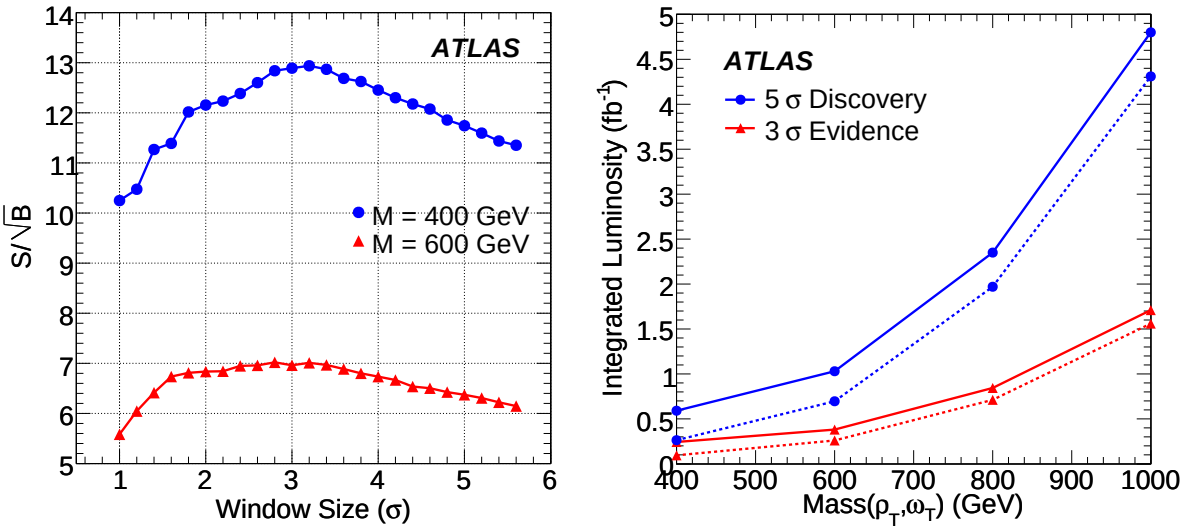

Figure 14: Left: for two different ρ_T, ω_T signal masses, $S/\sqrt{B}$ is plotted as a function of mass-window size for windows centered on the peak mass. Right: integrated luminosity needed for 3σ evidence or 5σ discovery as a function of ρ_T, ω_T mass. The dashed lines include only statistical uncertainties while the solid lines contain the systematic uncertainties as well.

6 Summary and Conclusions

Several models which lead to resonances in the dilepton final state have been studied. Various systematic studies have been undertaken which estimate the effect of uncertainties from both theoretical knowledge of Standard Model processes as well as expected and assumed early detector performance. Data-driven methods have been developed to evaluate efficiencies, backgrounds, and uncertainties. It has been shown that even with early data the discovery potential can be dramatically increased from current limits. The discovery potential with an integrated luminosity of 10 fb^{-1} depends on the particular model and varies in the $m = 1.0$ to 3.5 TeV range. It should be noted that resonance masses above 1 TeV which are unreachable by the Tevatron experiments could be discovered with 100 pb^{-1} of data already.

Acknowledgements

We thank B. Fuks and M. Klasen for their major contribution to section 4.2.

A Effect of the Unknown Location and Rate

When estimating the significance of a local excess of events, the size of the region considered and uncertainties in the shape of the background can significantly reduce the sensitivity of the search. This appendix presents an assessment of the size of this effect for the Z' boson to dilepton searches. If an excess is found in the dilepton invariant mass, its significance needs to be evaluated in a way that takes into account the possibility of background fluctuations of different masses, cross-sections and widths. One possible way to do this is through the use of maximum likelihood fits, where these quantities are free parameters.

To estimate the effect on the sensitivity of the unknown rate and location of a dilepton resonance, the decay $Z'_{SSM} \to ee$ and $Z'_{SSM} \to \mu\mu$ were both generated for 16 true Z' masses between 1 and 4 TeV (evenly spaced every 200 GeV), with a lower cut on the true dilepton mass of 0.5 TeV in all cases. Each sample was simulated and reconstructed using fast simulation, and events were required to have two back-to-back ($\Delta\phi > 2.9$) leptons of opposite charge with $p_T > 20$ GeV and within $|\eta| < 2.5$. For an estimation of the expected background, Standard Model Drell-Yan production was used.

The dilepton resonance was modeled using an ad-hoc parameterization that models appropriately the shapes of both the $Z' \to ee$ and $Z' \to \mu\mu$ modes, consisting of a product between a Breit-Wigner and a Landau distribution with a common mean, and where the width of the Landau was parameterized as a function of the width of the Breit-Wigner[10]. The common mean, the width parameter and the amplitude of the signal are allowed to float in the fits.

Figure 15 shows the likelihood ratio distributions for an $m = 3$ TeV $Z'_{SSM} \to ee$ fit-based significance, where the signal rate, the peak's width and the mean mass all float in the fit, corresponding to an integrated luminosity of 4 fb^{-1}. The distributions of the log-likelihood ratio for fits to H0 pseudo-experiments and for fits to H1 pseudo-experiments are shown. The fraction p of the H0 distribution that has a likelihood ratio larger than the mean of the H1 distribution is shaded. The value of p is then transformed into a significance following the convention under which $p = 2.87 \times 10^{-7}$ corresponds to 5σ (see section 5). The fraction shown in the plot corresponds to a significance of 4.29σ.

Several million pseudo-experiments were generated and fit, covering different masses and luminosities. Figure 16 shows the significance for different approaches in the case of an $m = 3$ TeV Z'_{SSM} for

[10] The best motivated shape is a Breit-Wigner convoluted with a Gaussian resolution. Unfortunately, the convolution fit is very time consuming and for this study millions of fits were performed. Empirically the combination of a Breit-Wigner and a Landau were found to give essentially identical results.

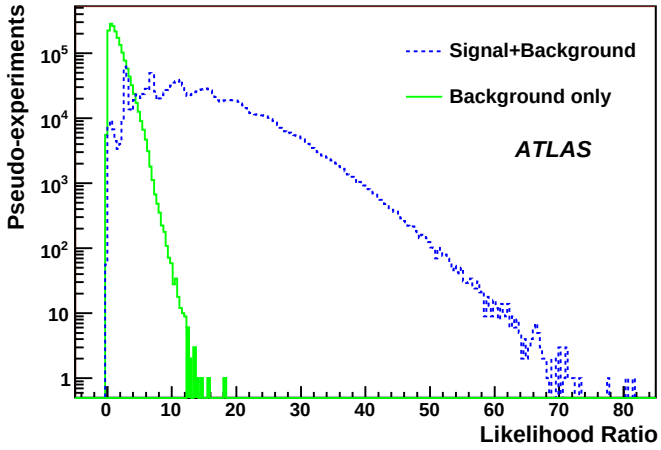

Figure 15: Likelihood ratio distribution for an $m = 3$ TeV $Z'_{SSM} \to ee$; the distribution on the left corresponds to background-only pseudo-experiments; the one on the right, to signal plus background.

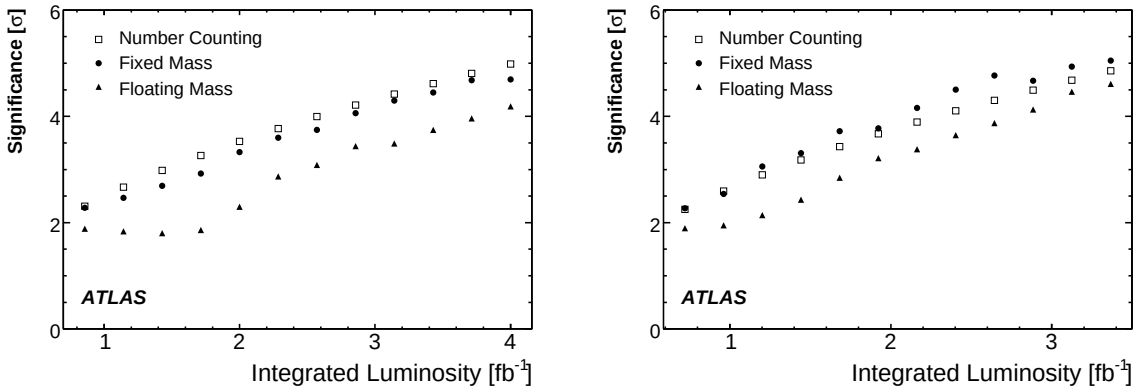

Figure 16: Comparison of the fit-based significance for fixed-mass (dots) and floating-mass (squares) fits for both cases, $Z' \to ee$ (left) and $Z' \to \mu\mu$ (right). Circles show the estimation from number counting.

both the dielectron (left) and the dimuon (right) cases. The plots compare the significance as obtained from number counting (circles), fixed mass fits (dots) and floating mass fits (squares). The floating-mass significances are on average 20% lower than the fixed-mass calculations for $Z' \to ee$, and about 15% lower in the dimuon case (in obtaining these numbers, we exclude the region below 2.25 fb^{-1}, which is affected by low statistics effects).

References

[1] H. Georgi and S. L. Glashow, *Phys. Rev. Lett.* **32** (1974) 438–441.

[2] K. D. Lane and E. Eichten, *Phys. Lett.* **B222** (1989) 274.

[3] N. Arkani-Hamed, A. G. Cohen, and H. Georgi, *Phys. Lett.* **B513** (2001) 232–240.

[4] L. Randall and R. Sundrum, *Phys. Rev. Lett.* **83** (1999) 3370–3373.

[5] **D0** Collaboration, V. M. Abazov *et al.*, *Phys. Rev. Lett.* **95** (2005) 091801.

[6] **CDF** Collaboration, A. Abulencia *et al.*, *Phys. Rev. Lett.* **96** (2006) 211801.

[7] **CDF** Collaboration, "High-Mass Dielectron Resonance Search in $p\bar{p}$ Collisions at $\sqrt{s}$ = 1.96 TeV." CDF/PUB/EXOTIC/PUBLIC/9160, 2008.

[8] F. Ledroit, J. Morel, and B. Trocmé, "Z' at the LHC." ATL-PHYS-PUB-2006-024, 2006.

[9] M. Cvetic, P. Langacker, and B. Kayser, *Phys. Rev. Lett.* **68** (1992) 2871–2874.

[10] **Particle Data Group** Collaboration, W. M. Yao *et al.*, *J. Phys.* **G33** (2006) 1–1232.

[11] P5-Committee, "The case for run II: Submission to the particle physics project prioritization panel. the CDF and D0 experiments." 2005.

[12] K. D. Lane, *Phys. Rev.* **D60** (1999) 075007.

[13] K. Lane and S. Mrenna, *Phys. Rev.* **D67** (2003) 115011.

[14] **CDF** Collaboration, A. Abulencia *et al.*, *Phys. Rev. Lett.* **95** (2005) 252001, `arXiv:hep-ex/0507104`.

[15] **ATLAS** Collaboration, "Reconstruction and Identification of Electrons." This volume.

[16] **ATLAS** Collaboration, "The ATLAS Experiment at the CERN Large Hadron Collider." JINST 3 (2008) S08003.

[17] **ATLAS** Collaboration, "The ATLAS Muon Spectrometer Technical Design Report." 1997.

[18] **ATLAS** Collaboration, "Muon Reconstruction and Identification: Studies with Simulated Monte Carlo Samples." This volume.

[19] **ATLAS** Collaboration, "Reconstruction and Identification of Hadronic τ Decays." This volume.

[20] **ATLAS** Collaboration, "Trigger for Early Running." This volume.

[21] **ATLAS** Collaboration, "Performance of the Muon Trigger Slice with Simulated Data." This volume.

[22] T. Sjöstrand, S. Mrenna, and P. Skands, *JHEP* **0605** (2006) 026.

[23] U. Baur, O. Brein, W. Hollik, C. Schappacher, and D. Wackeroth, *Phys. Rev. D* **65** (2002) 033007.

[24] V. A. Zykunov, *Phys. Rev. D* **75** (2007) 073019.

[25] A. D. Martin, R. G. Roberts, W. J. Stirling, and R. S. Thorne, *Eur. Phys. J. C* **39** (2005) 155.

[26] C. Glosser, S. Jadach, B. F. L. Ward, and S. A. Yost, *Mod. Phys. Lett. A* **19** (2004) 2113.

[27] C. M. C. Calame, G. Montagna, O. Nicrosini, and A. Vicini, *JHEP* **0710** (2007) 109.

[28] U. Baur, S. Keller, and W. K. Sakumoto, *Phys. Rev. D* **57** (1998) 199.

[29] G. Altarelli, R. K. Ellis, and G. Martinelli, *Nucl. Phys. B* **157** (1979) 461.

[30] R. Hamberg, W. L. van Neerven, and T. Matsuura, *Nucl. Phys. B* **359** (1991) 343. Erratum-ibid. *B* 644:403, 2002.

[31] C. Anastasiou, L. J. Dixon, K. Melnikov, and F. Petriello, *Phys. Rev. D* **69** (2004) 094008.

[32] A. Kulesza, G. Sterman, and W. Vogelsang, *Phys. Rev. D* **66** (2002) 014011.

[33] B. Fuks, M. Klasen, F. Ledroit, Q. Li, and J. Morel, *Nucl. Phys.* **B797** (2008) 322–339.

[34] S. Frixione and B. R. Webber, *JHEP* **0206** (2002) 029.

[35] P. Mathews, V. Ravindran, and K. Sridhar, *JHEP* **0510** (2005) 031.

[36] Q. Li, C. S. Li, and L. L. Yang, *Phys. Rev. D* **74** (2006) 056002.

[37] J. Bijnens, P. Eerola, M. Maul, A. Møansson, and T. Sjöstrand, *Phys. Lett. B* **503** (2001) 341.

[38] J. Pumplin *et al.*, *JHEP* **07** (2002) 012.

[39] W. K. Tung, H. L. Lai, A. Belyaev, J. Pumplin, D. Stump, and C. P. Yuan, *JHEP* **0702** (2007) 053.

[40] F. Petriello and S. Quackenbush, *arXiv:0801.4389 [hep-ph]* .

[41] G. A. Ladinsky and C. P. Yuan, *Phys. Rev. D* **50** (1994) 4239.

[42] F. Landry, R. Brock, P. M. Nadolsky, and C. P. Yuan, *Phys. Rev. D* **67** (2003) 073016.

[43] A. V. Konychev and P. M. Nadolsky, *Phys. Lett. B* **633** (2006) 710.

[44] T. Junk, *Nucl. Instrum. Meth.* **A434** (1999) 435–443.

[45] H. Hu and J. Nielsen, `arXiv:physics/9906010`. `http://www.citebase.org/abstract?id=oai:arXiv.org:physics/9906010`.

[46] **CMS** Collaboration, G. L. Bayatian *et al.*, *J. Phys.* **G34** (2007) 995–1579.

[47] G. Altarelli, B. Mele, and M. Ruiz-Altaba, *Z. Phys.* **C45** (1989) 109.

[48] **ATLAS** Collaboration, "Measurement of Missing Tranverse Energy." This volume.

[49] **CDF** Collaboration, D. E. Acosta *et al.*, *Phys. Rev. Lett.* **95** (2005) 131801.

[50] E. Eichten and K. Lane, `arXiv:0706.2339 [hep-ph]`.

[51] K.-M. Cheung and G. L. Landsberg, *Phys. Rev.* **D62** (2000) 076003.